Acta Cryst. (1999). A**55**, 168–177

Boron nitride cones: structure determination by transmission electron microscopy

Laure Bourgeois, Yoshio Bando, Satoshi Shinozaki, Keiji Kurashima and Tadao Sato

National Institute for Research in Inorganic Materials, Namiki 1-1, Tsukuba, Ibaraki 305-0044, Japan

(*Received 15 March 1998; accepted 22 June 1998*)

Dedicated to Professor A. F. Moodie on the occasion of his 75th birthday

Abstract

A form of turbostratic boron nitride containing a large percentage of micrometre-size conically shaped particles was investigated by transmission electron microscopy. Electron diffraction patterns revealed the presence of correlations between adjacent boron nitride layers. The diffraction patterns were also used to determine the cone apex angle of many cone-like objects. The apex angles exhibited a broad distribution from 84 to 130° with an ill defined peak in the 92–95° region. These results could be accounted for by a structure model in which conical boron nitride layers are helically wound about a disclination axis, according to overlap angles that correspond to high densities of coincidental lattice sites between successive layers. The clustering of the apex angles near 93° was attributed to the formation of a square ring during the nucleation stage. This appears to be specific to the boron nitride system.

1. Introduction

The growth of novel boron nitride (BN) whiskers has recently attracted attention, in particular from the perspective of synthesizing nanotubes and fullerene particles. This interest has been motivated by the structural resemblance between boron nitride and carbon, the carbon system being well known for its nanotubules (Iijima, 1991) and the fullerene family (Kroto *et al.*, 1985). More specifically, theoretical studies have shown that, contrary to carbon, BN nanotubes should exhibit electronic properties that are fairly independent of the tube's geometry, making such material more useful for potential applications (Rubio *et al.*, 1994; Blase *et al.*, 1994).

A tubular form of amorphous BN analogous to the carbon fibres discovered by Bacon (1960) was first synthesized by Hamilton *et al.* (1993). Later, pure BN nanotubes were fabricated using a variety of techniques (Chopra *et al.*, 1995; Loiseau *et al.*, 1996; Golberg *et al.*, 1996). In most cases, tube caps were either absent or flat, suggesting that the formation of pentagons might be unfavourable in the hexagonal (*h*-) BN lattice. This is thought to be the consequence of the higher stability of B—N bonds relative to B—B and N—N bonds (Loiseau *et al.*, 1996).

Despite the relative ease with which BN nanotubes were discovered, the synthesis of their buckyball equivalent is still proving elusive. Recently, Stéphan *et al.* (1997) reported the formation of BN analogues to small single-layer and nested fullerene cages following intense electron irradiation of *h*-BN in the electron microscope. The polygonization observed for some of the larger onion-like particles was compatible with theoretical models proposed by Jensen & Toftlund (1993) and Seifert *et al.* (1997), again pointing to square-ring defects instead of pentagons (Stéphan *et al.*, 1997). However, direct evidence for (or against) the existence of squares in the BN hexagonal lattice is still lacking.

Like graphite, BN has been known for some time to form whiskers displaying a variety of unusual shapes. Examples of this are the filamentary crystals reported by Ishii *et al.* (1981). More recently, a type of turbostratic BN examined under scanning electron microscopy was found to consist of columnar particles with conical tips (Sato, 1996). These particles were separated by heat treatment from a B–C–N material also containing carbon cones (Sato, 1996). Carbon particles consisting of conical helically wrapped graphitic layers have already been studied by several authors (Haanstra *et al.*, 1972; Double & Hellawell, 1974; Amelinckx *et al.*, 1992). The cones were found to have specific apex angles and hence disclination angles – the disclination angle is defined as the angle of the sector removed from a flat sheet to form the cone – which were ascribed to high densities of coincidental lattice sites between overlapping layers. For a honeycomb array, there are several configurations achieving optimum coincidence. These correspond to disclination angles that are multiples of 60° in combination with values between 20 and 30° (Double & Hellawell, 1974; Amelinckx *et al.*, 1992). In the case of disclination angles, exactly equal to $60n^\circ$ (where n is a positive integer between 1 and 5), a closed (*i.e.* nonhelical) monolayer cone can form with a $(6-n)$-membered ring as its only defect. Note that in helical cones the disclination is associated with a screw rotation operation, whereas in nonhelical cones the disclination is a purely rotational defect. Graphitic cones exhibiting the whole range of pure $60n^\circ$ disclinations have also

ISSN 0108-7673

been reported by Krishnan *et al.* (1997). The $60n^\circ$ disclinations observed by Krishnan *et al.* (1997) were probably composed of n pentagons instead of a single $(6-n)$-membered ring, as the former configuration results in far less strain in the structure.

Therefore, conical structures of layered compounds are worth investigating as they originate from a single defect in the two-dimensional lattice, and hence can provide information about the formation probability of $60n^\circ$ disclinations, which is of particular use for the study of potential BN fullerenes. This was our prime motivation for undertaking a transmission-electron-microscopy study of these novel BN structures.

In the present work, we show that the turbostratic BN particles are helically wrapped cones and that they bear a strong resemblance to the graphitic cones investigated previously (Haanstra *et al.*, 1972; Double & Hellawell, 1974; Amelinckx *et al.*, 1992). In particular, cone apex angles are determined by very similar coincidental lattice site configurations. However, the clustering of cone-angle values around 94° observed in BN cones is found to be specific to the BN system. It is attributed to the lower energy of square rings compared with pentagons.

2. Experimental details

Turbostratic boron nitride (*t*-BN) was obtained by separating a B–C–N material (Sato, 1996) prepared by heating a fused mixture of boric acid, urea and saccharose (Hubáček & Sato, 1995). X-ray diffraction showed the compound to consist of equidistant *h*-BN sheets separated by a distance of 3.46 Å (compared with 3.33 Å for crystalline *h*-BN), which implies weak inter-sheet correlations. The two-dimensional ordering of individual layers was nevertheless found to be very high. This material was named βt-BN to distinguish it from another *t*-BN compound (αt-BN) characterized by disorder in the stacking sequence of the layers only (Sato, 1996). Scanning electron microscopy (SEM) of βt-BN revealed the presence of large column-shaped particles (Sato, 1996), which are the subject of the present TEM study. Objects having this columnar morphology were also observed in the carbon material separated from βt-BN in B–C–N (Sato, 1996). A TEM investigation of this material will be reported in a forthcoming article (Bourgeois *et al.*, 1999).

βt-BN, which takes the form of a dark grey powder, was crushed in an agate mortar and sonicated in CCl_4 for about one minute before being mounted onto a carbon-film-coated copper grid for viewing in the transmission electron microscope. TEM observations were carried out on a field emission JEOL 3000F analytical microscope operated at 300 kV and equipped with a ±30° tilting stage. The elemental composition and chemical bonding of the objects under examination could be probed by means of electron-energy-loss spectroscopy (EELS) using a Gatan parallel EELS detector.

Finally, beam damage and contamination were found to be minimal even after several minutes of observation.

3. Results and analysis

βt-BN was found to be composed of micrometre-size particles, which EELS analysis showed to consist solely of sp^2-bonded BN with no measurable traces of carbon,

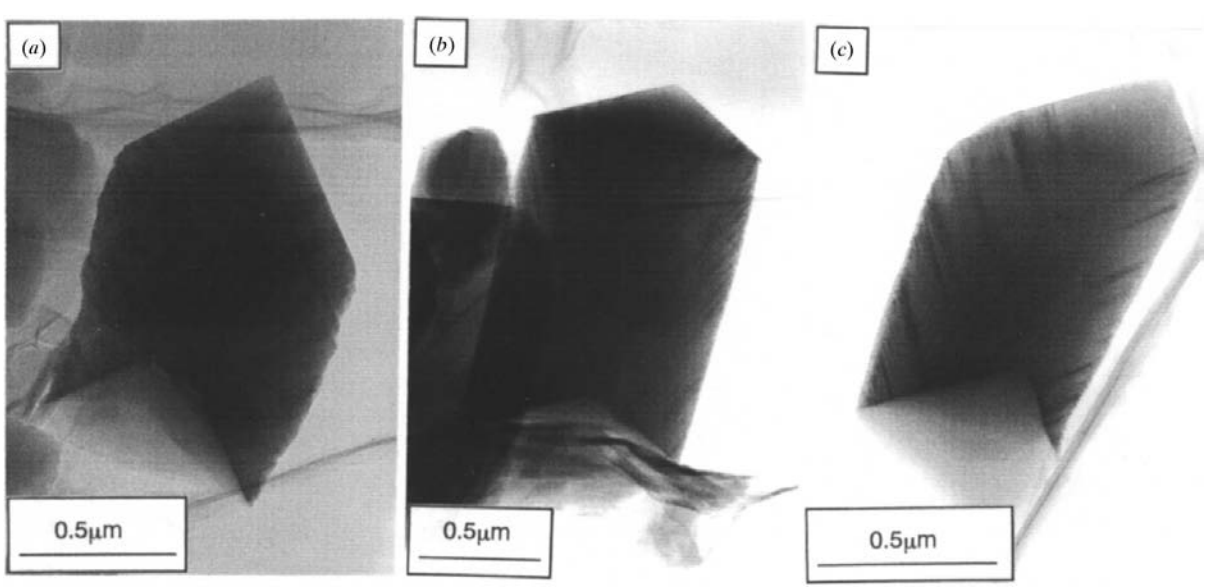

Fig. 1. Low-magnification TEM images showing three examples of arrow-shaped particles. The angle of the "arrow's" tip can vary significantly, from less than 90° (*a*) to about 130° (*b*). Angle values between 90 and 100° as in (*c*) were by far the most common.

i.e. less than a few percent. A significant proportion of the particles exhibits a characteristic arrow-like shape. In Fig. 1, a variety of such objects are displayed. Note in particular the different angles of the "arrow's" tip, from less than 90° in (*a*) to about 130° in (*b*). Tip angles between 90 and 100° such as in (*c*) were found to be by far the most common.

Another similar but thinner object is selected in Fig. 2(*a*), together with high-resolution (HR) micrographs of its tip (*c*) and of the bottom part of one of the two 'wings' (*d*). The image of the tip (*c*) shows two sets of stacked parallel layers meeting at a sharp angle. The parallel fringes are well defined throughout the image (except at the intersection zone, where contrast is

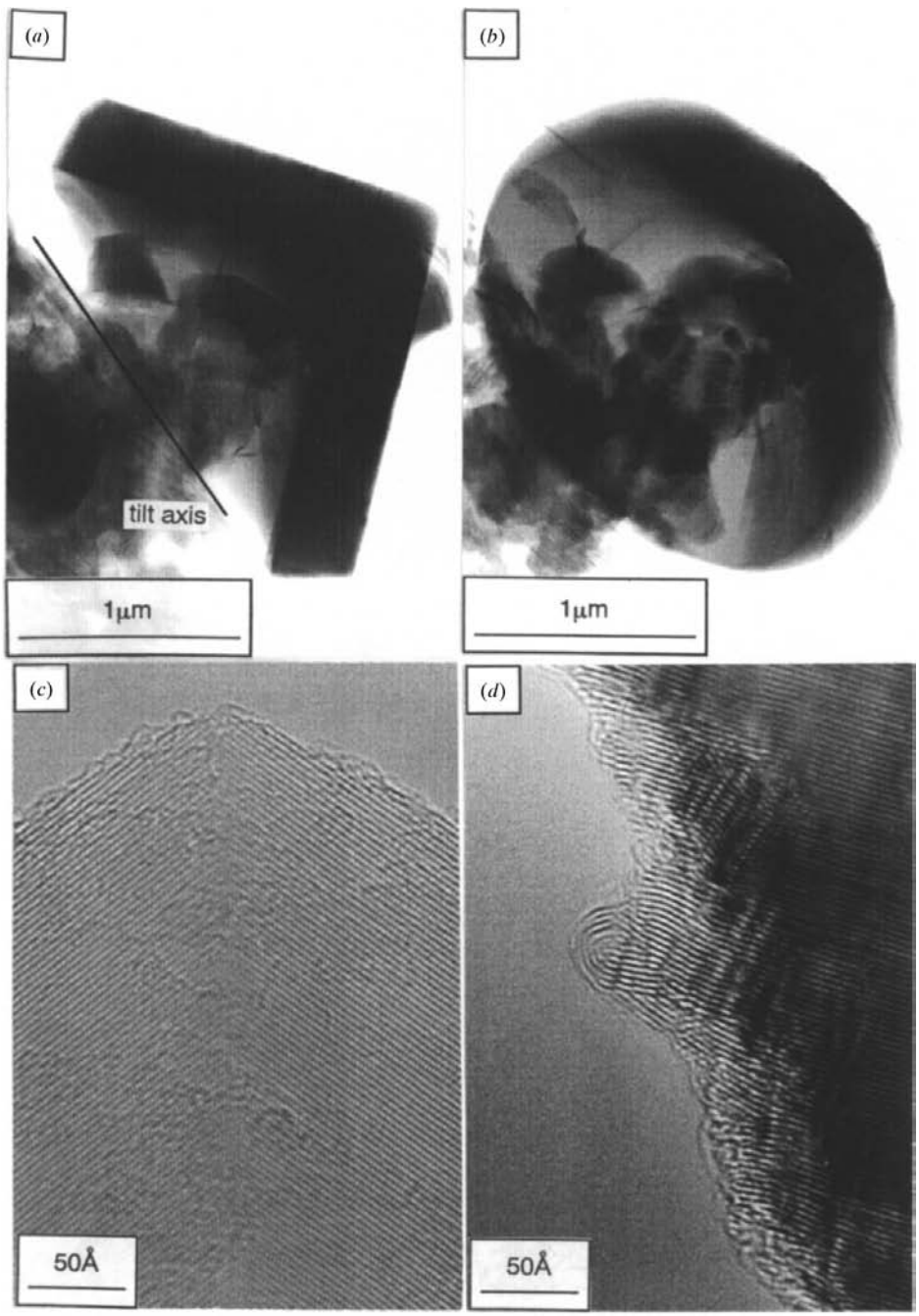

Fig. 2. (*a*) Arrow-shaped object (*b*) tilted some 30° about the axis shown in (*a*). In (*b*), the conical morphology of the particle is clearly visible. Higher-magnification images of the tip and wing regions of a similar object are shown in (*c*) and (*d*), respectively.

weaker), indicating a high degree of two-dimensional order. An average interlayer spacing of 3.48 (5) Å was measured from electron diffraction patterns. This is in agreement with the value of 3.46 Å estimated from X-ray diffraction for the bulk βt-BN material (Sato, 1996).

The object of Fig. 2(*a*) gets progressively thicker away from its centre. In Fig. 2(*b*), the particle is tilted ~28° with respect to (*a*) about the axis shown in the picture; the rounded shape of the 'arrow' is now apparent. Hence, there is little doubt that the arrow-shaped objects have a conical shape, which confirms the SEM observations (Sato, 1996). Two possible structure models are proposed in Fig. 3. In (*a*), monolayer BN cones stack on top of each other turbostratically; in (*b*), the sheet does not close to form a conical 'hat' as in (*a*), but rather overlaps itself in a helical fashion. The true and observed cone apex angles, θ_{apex} and θ_{obs}, respectively, are defined in Fig. 3(*a*). The entire object constituted of stacked-up or helically wound BN conical sheets will now be called a BN cone.

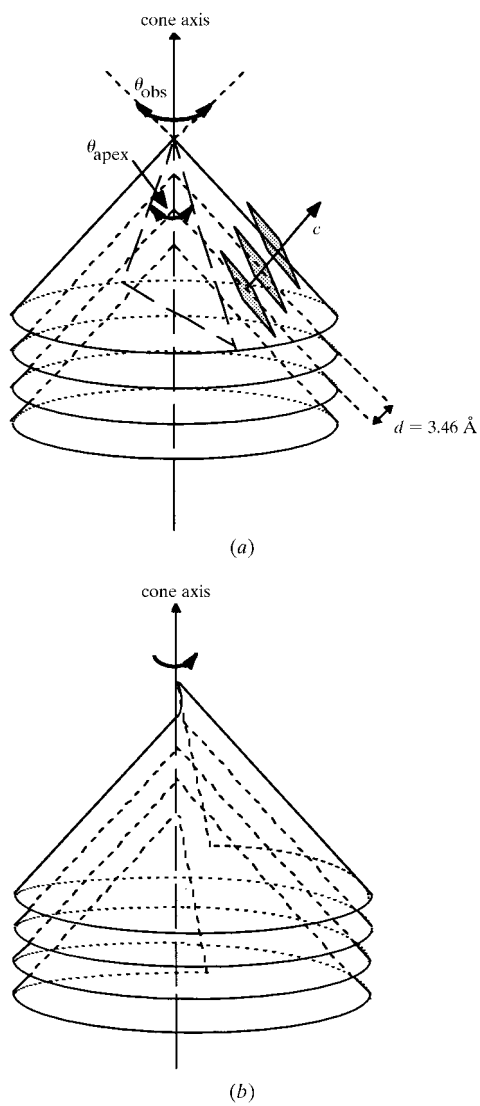

Fig. 3. Models proposed for the particles shown in Figs. 1 and 2. (*a*) Piled up conical *h*-BN monolayers. (*b*) Conical helically wound BN layer. In (*a*) a volume element is shown with its local normal.

The more or less circular edges of the BN cone sometimes join as curved or polygonized sections (see Fig. 2*d*), presumably in order to eliminate unsaturated bonds as is often the case in graphitic like particles. But this 'onion' feature is far from common, as Fig. 2(*d*) shows.

There is some amorphous material visible on the outer surface of the cones. But from the difference in contrast between the central and bottom sections of the particles, the bottom cone can be deduced to be empty [apart from various small objects in Fig. 2(*a*), which probably entered the cone after it was formed].

The number of stacked layers was observed to be very large, typically at least several hundred. Thinner BN cones containing about 50 layers were found in the specimen. However, they were all seriously damaged, usually flattened and folded.

At this stage, it is difficult to decide which of the two suggested structure models of Fig. 3 fits the observed cones better. Hence, a careful study of the cone-apex-angle distribution was carried out in order to gain more information about the apical region of the cones, and more specifically about the associated rotation defect(s). Because the length of BN cones was often not uniform [see Fig. 1(*c*) for example], the deprojection method used by Krishnan *et al.* (1997) to deduce the apex angles would be unreliable here. Since the arrow shape of a BN cone with its cone axis lying approximately perpendicular to the incident electron beam reflects the layer stacking closely, the most direct method is to tilt the object until its projected (or observed) apex angle θ_{obs} is minimized, in which case it is equal to the true apex angle, θ_{apex}. Unfortunately, this is a time-consuming procedure if reasonably accurate values (*i.e.* within 1 or 2°) are to be obtained. However, the value of the true apex angle can be derived from a diffraction pattern of the tip of the BN cone, as will be demonstrated in the following. The object only requires to have its cone axis roughly perpendicular to the incident beam and the uncertainty of the measured value for θ_{apex} is only 1°.

In order to understand how information about the apex angle can be obtained from a diffraction pattern, the reciprocal-space structure of a BN cone must be known. The detailed geometry of the diffraction space associated with a conical sheet was determined by Amelinckx *et al.* (1996) in their study of helically rolled conical chrysotile structures. Here we will limit ourselves to stressing the features of a cone's reciprocal space that are relevant to obtaining the apex angle. A reciprocal-space construction for an ideal (*i.e.* unfaceted and non-helical) layered cone such as drawn in Fig. 3(*a*) is shown

in Fig. 4. For the sake of simplicity, no correlation in orientation between adjacent BN sheets are assumed, and so only the 000*l* and *hk*.0 reflections need to be examined. This assumption appears reasonable in the view of the large interlayer spacing measured, which indicates that correlations are weak.

First we treat the 000*l* reflections. To each volume element such as sketched in Fig. 3(*a*) will correspond in reciprocal space a set of (000*l*) nodes along the local normal to the planes, *i.e.* along the reciprocal vector $\mathbf{c}^*$ (see Fig. 4*a*). Rotation of these nodes about the cone axis will yield the (000*l*) reciprocal-space locus for the entire object: circles C_{000l} located equidistantly on a quadratic cone of angle $180 - \theta_{\text{apex}}$ (see Fig. 4*b*). These circles have radius $r_{000l} = g_{000l} \sin(\theta_{\text{apex}}/2)$ and their respective centres are separated by a distance g_{0002},

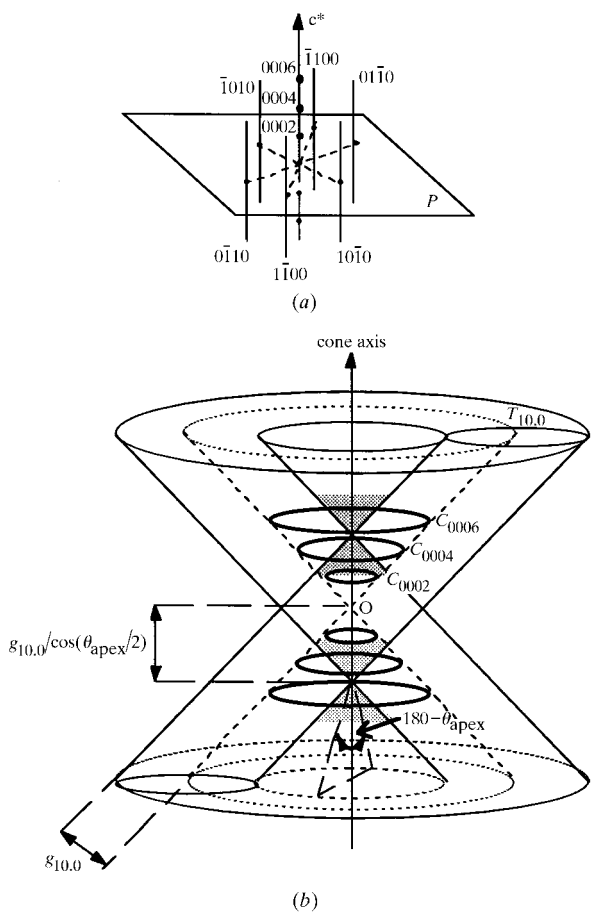

Fig. 4. Reciprocal-space construction (*a*) for a small volume element as in Fig. 3(*a*), showing the (000*l*) nodes along the local normal (which is parallel to the reciprocal vector $\mathbf{c}^*$), and *hk*.0 streaks arranged in a hexagonal array (shown for one sheet only, parallel to plane *P*); (*b*) for the volume element rotated about the cone axis. The (000*l*) locus lies on the cone drawn as dashed lines. The (*hk*.0) locus is a cylinder (radius $g_{hk.0}$ and needle axis tilted by $90 - \theta_{\text{apex}}/2$ with respect to the cone axis) rotated about the cone axis. One such cylinder is drawn, together with the double conical envelop of the (*hk*.0) locus (solid line).

where $g_{hk.l}$ is the length of the diffraction vector taken between the origin *O* and the reflection *hk.l*.

hk.0 reflections will now be considered. The reciprocal space for a single layer of the volume element shown in Fig. 3(*a*) is a hexagonal array perpendicular to the local normal to the sheet. Since no correlations between adjacent sheets are assumed, each (*hk*.0) node will be a long streak along the local normal, *i.e.* along the row of (000*l*) nodes (see Fig. 4*a*). For a large number of layers in the volume element, the geometrical locus for a given (*hk*.0) node is a cylinder $T_{hk.0}$ of radius $g_{hk.0}$ and needle axis parallel to the local normal. Now each cylinder should be rotated about the cone axis to give the (*hk*.0) locus for the entire BN cone. Each *hk*.0 streak is then associated with a cone with angle equal to $180 - \theta_{\text{apex}}$ and with its apex situated at a distance $g_{hk.l}/\cos(\theta_{\text{apex}}/2)$ from the origin *O*. In Fig. 4(*b*), only two cones corresponding to the two opposite sides of a $T_{10.0}$ cylinder are sketched for clarity. However, one must imagine that each 000*l* row is the axis of a set of $T_{hk.0}$ cylinders. Note that the above is only valid for volume elements that are far enough from the apex of the cone, *i.e.* for regions whose radius of curvature is much larger than the interatomic spacing.

The general features of the electron diffraction patterns expected from a BN cone can now be established. For a given direction of the incident electron beam, the reflections are given by the intersection between the Ewald sphere and the reciprocal lattice described above. Owing to the large size of the cone particles, good diffraction patterns could only be obtained when the object had its cone axis more or less perpendicular to the incident beam, *i.e.* in the orientation of Fig. 2(*a*) rather than of Fig. 2(*b*). In that configuration, the Ewald sphere – a plane to a very good approximation – is more or less tangent to the cone axis. The case of the Ewald plane exactly parallel to the cone axis is shown in Fig. 5(*a*) together with an electron diffraction pattern obtained experimentally when the observed apex angle θ_{obs} is minimized, *i.e.* when $\theta_{\text{obs}} = \theta_{\text{apex}}$ (θ_{obs} is the angle between the 000*l* fringes on a high-resolution image of the tip region). The particle from which the diffraction pattern was taken was measured to have $\theta_{\text{apex}} = \theta_{\text{obs}} = 94\,(1)^\circ$. In that case, the intersection of the Ewald sphere with the C_{000l} circles consists of two rows of 000*l* reflections meeting at an angle equal to $180 - \theta_{\text{apex}}$ (°). The intersection with the (*hk*.0) locus results in *hk*.0 arcs along the direction perpendicular to the cone axis (which is also the *y* axis shown on the diffraction pattern) and sets of hyperbola-like curves $H_{hk.0}$ with their vertices along the *y* axis. The maximum distance between the vertices of the $H_{hk.0}$ curves is equal to $2g_{hk.0}/\cos(\theta_{\text{apex}}/2)$. In Fig. 5(*a*), only the 10.0 reflections and one set of $H_{10.0}$ curves are shown. Fig. 5(*a*) indicates that the predicted diffraction pattern accounts well for the overall shape of a diffraction pattern obtained experimentally by mini-

mizing the projected apex angle θ_{obs}. More importantly, the apex angle deduced from the diffraction pattern is 93.9 (7)°, in agreement with the value measured directly from the image.

When the cone axis is not perpendicular to the incident electron beam, θ_{obs} is larger than θ_{apex}. This is reflected in a change in angle between the (000*l*) rows. The intersection of the Ewald sphere with the cones of the reciprocal lattice will also result in two characteristic separations between the hyperbola-like curves, as illustrated in Fig. 5(*b*). These two distances in effect correspond to the two different angles θ_1 and θ_2 between the incident beam and opposite sides of the conical object. θ_1 and θ_2 can be calculated from the relationship $\theta_j = \arccos(2g_{hk.0}/g_j)$, where $j = 1$ or 2, g_j is the minimum or maximum separation between curves $H_{hk.0}$ and $g_{hk.0}$ is the diffraction vector of the *hk*.0 reflection. $g_{hk.0}$ is half the separation of the *hk*.0 arcs, which remains unchanged with tilting. The sum $\theta_1 + \theta_2$ is then equal to θ_{apex}. From the experimental diffraction pattern of Fig. 5(*b*), $\theta_1 = 42.4\,(7)^\circ$ and $\theta_2 = 51.3\,(7)^\circ$, hence $\theta_{apex} = 94\,(1)^\circ$. This agrees with the direct measurement of θ_{apex} as well as with the value obtained from Fig. 5(*a*). The uncertainty arising from the measurements of $g_{hk.0}$ and g_j on the diffraction pattern was estimated to be 1° for $\theta_{apex} < 100^\circ$ (approximately). For larger values of the apex angle, the distance g_j becomes very large and the corresponding reflections are quite faint, thus inducing a larger error, typically 2°. In these cases, we had to resort to measuring θ_{apex} directly from the image. Values for θ_{apex} can then be obtained for a variety of orientations of the BN cone with respect to the incident electron beam, provided the cone axis is within about 15° of being perpendicular to the incident-beam direction, otherwise the $H_{hk.0}$ curves furthest away from the origin are too faint. The θ_{apex} results were found: (i) to agree within uncertainty margins with the value directly measured on the high-resolution image from $\theta_{obs} = \theta_{apex}$ when θ_{obs} is minimized; (ii) to remain constant over the range of orientations attainable with the tilting sample holder. The second point confirms the perfectly conical morphology of the BN cones, and in particular the very low degree of faceting present in the structure. Point (i) indicates that a BN cone need not be aligned exactly

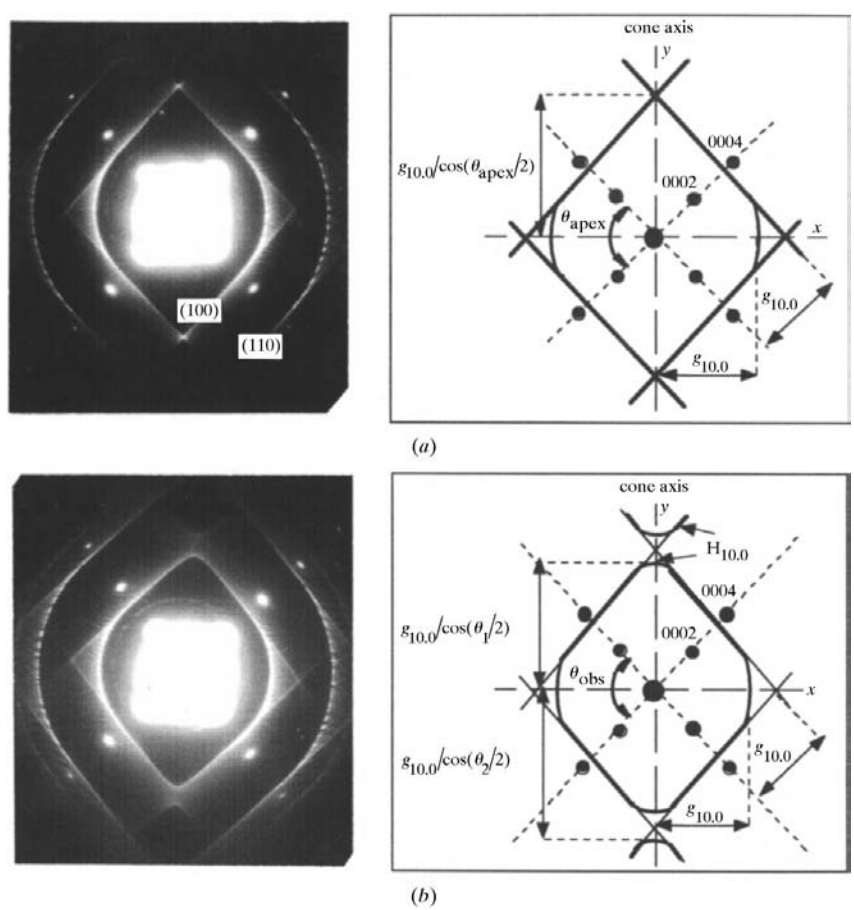

Fig. 5. Experimental diffraction patterns of a BN cone (tip region): (*a*) when the apparent apex angle θ_{obs} is minimized; (*b*) when the apparent apex angle θ_{obs} is about 2° from its minimum value θ_{apex}. Each diffraction pattern is interpreted with the help of the reciprocal-space structure of Fig. 4. The cone apex angle was measured to be 94° from these diffraction patterns. See text for more details.

with its axis perpendicular to the incident beam for its apex angle to be measured. Hence, this method allows a much quicker determination of θ_{apex}.

Before the results for the apex angles are given, one should point out an important feature of the recorded diffraction patterns not predicted by the above rough description: the intensity of the *hk*.0 arcs is not uniform but tends to be concentrated in more or less periodic stripes. This discreteness is a sign that some degree of correlation between successive sheets actually exists. Whether these correlations play a significant role in the structure of the BN cones will be discussed shortly.

Values of θ_{apex} were obtained for 75 BN cones. The results are plotted in Fig. 6 in the form of a histogram. It shows a distribution of apex angles between 84 and 130°, with all values but four no larger than 107° and centred on 93–94°.

In this range of apex-angle values, only one can be attributed to a disclination allowed in a hexagonal net and with no screw operation associated. It is the smallest angle encountered in our specimen: 84°. Indeed, an apex angle of 83.6° corresponds to a 120° wedge disclination, *i.e.* disclination angle $D_\theta = 360[1 - \sin(\theta_{\text{apex}}/2)] = 120°$. Other screwless disclinations such as resulting from a single pentagon ($\theta_{\text{apex}} = 112.9°$) or rings smaller than a square ($\theta_{\text{apex}} < 83.6°$) were not seen. So the defect associated with the 120° disclination is probably a square-like defect and not a pentagon pair since a pentagon appears to be less favourable energetically. Interestingly, almost all the cones characterized by an apex angle less than about 88° exhibited some deformation of their apical region. This is in contrast to cones with larger θ_{apex}, which showed a highly ordered structure even very close to their axis, as made clear by the high-resolution picture of the cone-tip region (see Fig. 2*c*). This indicates that well defined defects must be responsible for the different apex angles observed. Besides, the relatively spread-out distribution of apex-angle values points to the existence of a variety of apical defects. These observations, added to the knowledge that the sheets present some degree of correlation, lead us to favour the cone-helix model sketched in Fig. 3(*b*). Thus, it would appear difficult for a single closed cone (or 'hat') to have apex angles intermediate between 84 and 113°, *i.e.* not corresponding to $60n°$ disclinations, without experiencing relatively large strain.

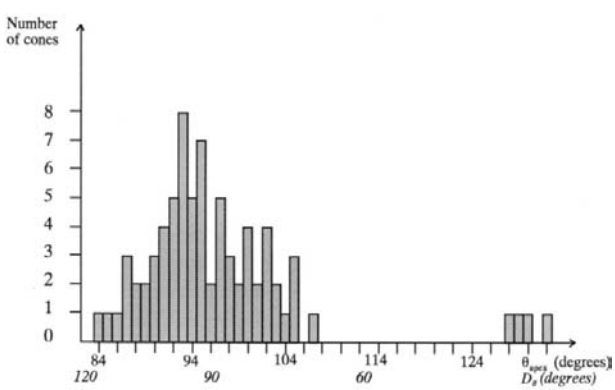

Fig. 6. Histogram of measured apex-angle values. The uncertainty on the measurements is 1°.

Table 1. *Combinations of overlap angles θ_{over} and multiples of 60° leading to disclination angles D_θ and cone apex angles θ_{apex} observed in βt-BN cones*

Disclination angle $D_\theta = 60n \pm \theta_{\text{over}}$ (°)	Cone apex angle θ_{apex} (°)
$60 - 27.7 = 32.3$	131.1
$60 - 24 = 36$	128.3
$60 - 21.7 = 38.3$	126.7
$60 + 10.4 = 70.4$	107.1
$60 + 13.1 = 73.1$	105.7
$60 + 15.1 = 75.1$	104.6
$60 + 21.7 = 81.7$	101.3
$60 + 24 = 84$	100.1
$60 + 27.7 = 87.7$	98.3
$120 - 27.7 = 92.3$	96.1
$120 - 24 = 96$	94.3
$120 - 21.1 = 98.3$	93.3
$120 - 15.1 = 104.9$	90.2
$120 - 13.1 = 106.9$	89.3
$120 - 10.4 = 109.6$	88.1
120	83.6

Overlapping hexagonal arrays with a common *c* axis tend to be oriented relative to each other according to specific rotation angles between 0 and 30°, ensuring highest density of coincidental lattice sites. These relative rotation angles were observed to be 22, 28 and 13° in overlapping *h*-BN platelets (Shimomura *et al.*, 1995). Other less common angles between 5 and 30° were also encountered. In a disclination of angle D_θ, a full 360° rotation about the disclination axis will cause atoms to rotate by an angle $|D_\theta - 60n|°$. Thus, if the conical sheet does not close upon itself but instead overlaps, the overlapping parts of the sheet will be rotated relative to each other by an angle $\theta_{\text{over}} = |D_\theta - 60n|°$. We will refer to θ_{over} as the overlap angle of the cone. Certain values of θ_{over} will result in a higher density of coincidental lattice sites and hence should be preferred. In previous studies, this model successfully explained why carbon cones exhibit apex angles corresponding to $\theta_{\text{over}} = 21.7$, 24 and 27.7°, which happen to be associated with the most favourable coincidence-lattice configurations in graphite (Double & Hellawell, 1974; Amelinckx *et al.*, 1992). Additional rotation angles (15.1, 13.1, 12, 10.4°) were suggested as possible, but they were not found in graphitic cones (Amelinckx *et al.*, 1992). Since combining these overlap angles with multiples of 60° does not alter the configuration of coincidental lattice sites, the whole range of apex angles in helical cones (from 0 to 180°) can be covered with this model. Table 1 shows the $D_\theta = (60n \pm \theta_{\text{over}})°$ combinations that can be attributed to the BN cones of the present study, with θ_{over} taking the values mentioned above. $\theta_{\text{over}} = 21.7$, 24

and 27.7° account for most of the particles observed, as was the case for carbon.

More details about the helical cone structure can be obtained from the fine structure of the electron diffraction patterns, as was demonstrated by Amelinckx *et al.*, 1992). Although diffraction patterns of the type shown in Fig. 5 are very useful in that they can yield the cone apex angle, their fine structure is difficult to interpret. On the other hand, diffraction patterns obtained when the incident electron beam is parallel to the *c* axis of the BN layers can provide information about intersheet correlations. In this orientation, diffraction patterns consist of concentric spherical rings. Just like in the diffraction patterns of Fig. 5, the rings are not continuous but present segmentation (Amelinckx *et al.*, 1992). The segmentation is not always periodic but often shows a clear multiplicity, from less than 20 to over 100. This pseudo-symmetry can be understood as the smallest number M of rotations of angle θ_{over} resulting in an integer multiple of 360°. In other words, $M\theta_{over} = k360°$, where k is a usually small positive integer (Amelinckx *et al.*, 1992). Hence, the pseudo-symmetry associated with a given cone should yield an overlap angle compatible with the apex angle. Fig. 7 shows diffraction patterns taken near the *c* zone axis of three different BN cones with known θ_{apex}. Measuring the apex angle requires the particles to have their cone axis more or less perpendicular to the incident beam, so getting the local *c* axis parallel to the beam would involve tilting the object by $\theta_{apex}/2$, which is not feasible with our ±30° tilting stage. Nonetheless, even when *c* is not quite aligned with the electron beam, the pseudo-symmetry characteristic of the cone is still clearly visible. The multiplicities observed in Fig. 7 are $M = 12$, 18 and 30 from (*a*) to (*c*). The corresponding cone angles were measured to be 97 (1), 102 (1) and 95 (1)°, respectively. Table 2 shows the overlap angles deduced from the values of M and the corresponding disclination and apex angles that fall closest to the measured θ_{apex}. Overlap angles determined from M can be seen to be entirely compatible with the experimental values of θ_{apex}. This is strong evidence in favour of the cone-helix model depicted in Fig. 3(*b*). One should also note the presence of θ_{over} values not reported for carbon cones, namely 30 and 20°. This may be due to the different stacking preferences of *h*-BN compared with graphite.

4. Discussion

The above electron-diffraction-pattern analysis has shown that the structure of BN cones presents many similarities with graphitic cones. Thus both BN and carbon cone particles consist of helically wound conical sheets. The apex angles of the cones are determined by almost the same specific overlap angles, 21.7, 27.7 and 24° being the most frequently encountered values. However, the range of apex and disclination angles was found to be quite different. In helical carbon cones, low disclination-angle values appeared to be preferred (*i.e.* $D_\theta = 0$–60°), whereas BN cone disclination angles were in the great majority between 72 and 120°. A preliminary investigation of the B–C–N compound containing both C and BN cones (Bourgeois *et al.*, 1999) confirmed this difference. This indicates that the present results are specific to BN cones and not to the experimental conditions during synthesis.

The clustering of most BN-cone θ_{apex} values above 83.6°, where the disclination defect is a square, leads us

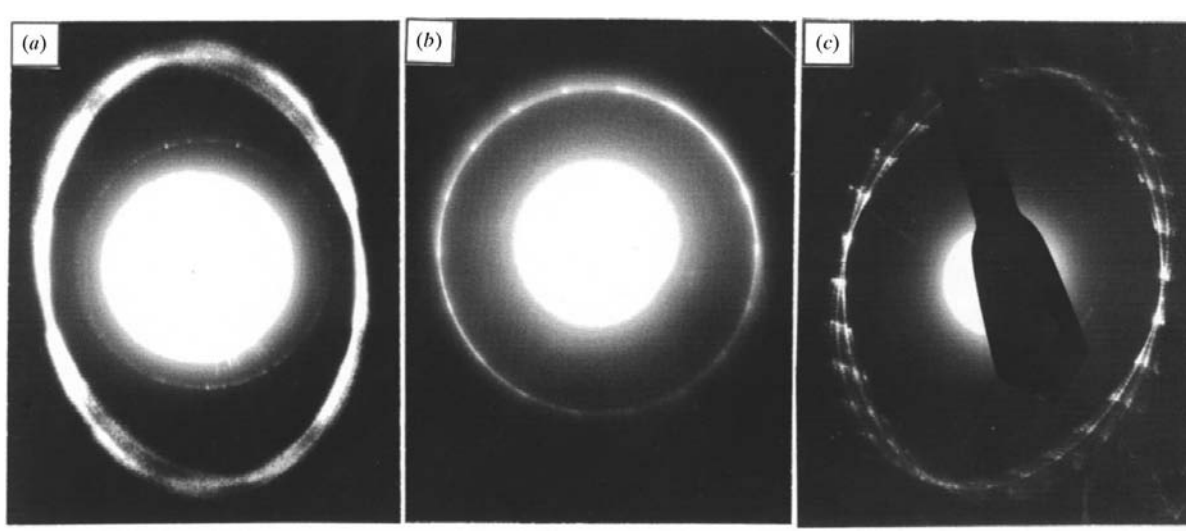

Fig. 7. Electron diffraction patterns taken near the (0001) zone axis of three different cone particles. The rings [only the (10.0) rings are shown] exhibit pseudo-symmetries M of 12, 18 and 30 from (*a*) to (*c*), respectively. The corresponding three cones have apex angles equal to (*a*) 97, (*b*) 102 and (*c*) 95°. Overlap angles calculated from the value of M lead to apex angles that are in excellent agreement with the measured values (see Table 2).

Table 2. *Multiplicities (or pseudosymmetries) observed in Fig. 7 for three cones whose apex angles were measured from diffraction patterns of the apical region*

Multiplicity M	Predicted $\theta_{over} = k360^\circ/M$	Predicted $D_\theta = 60n \pm \theta_{over}$	Predicted $\theta_{apex} = 2\arcsin(1 - D_\theta/360)$	Measured θ_{apex}
12	30° ($k = 1$)	90° ($n = 1$ or 2)	97.2°	97 (1)°
18	20° ($k = 1$)	$60 + 20 = 80^\circ$	102.1°	102 (1)°
30	12° or 24° ($k = 1$ or 2)	$120 - 24 = 96^\circ$	94.3°	95 (1)°

to propose that in βt-BN the nucleation of a proto-cone is associated with the formation of a square. The introduction of a square ring will force a small honeycomb sheet to adopt a conical shape. However, if one of the four bonds breaks or does not form at all, it will not be possible for the small BN sheet to close into a conical 'hat' without introducing many defects in its honeycomb array. On the other hand, overlapping itself will not present such problem. Moreover, the helical configuration will allow growth to proceed fairly easily, hampering any further rearrangement of the apical region of the cone, and hence keeping the total disclination angle in the vicinity of 120°. Therefore, our observations confirm that the square and not the pentagon is the most prevalent ring defect in BN. Nevertheless, the presence of a small percentage of cones near $\theta_{apex} = 130^\circ$ suggests that pentagons do form in BN, albeit very rarely. Indeed, the fact that the apex-angle region between 106 and 126° is empty favours the scenario of a pentagon forming and then giving rise to cones with $\theta_{apex} = 130^\circ$ rather than that of a proto-cone with a square-like defect subsequently opening up to exhibit a θ_{apex} much larger than 84°. If it were the case, one would expect cones to exhibit the full range of apex angles between 84 and 130°. It is also interesting to note that not a single particle with $\theta_{apex} < 84^\circ$ was observed. It may reflect excessive strain caused by a square. This has been conjectured before in order to explain the absence of well formed BN fullerene analogues (Banhart *et al.*, 1994) and is compatible with our observation that most cones with $\theta_{apex} < 88^\circ$ present signs of damage. However, this characteristic may also be due to growth conditions specific to our specimen. For instance, growth may proceed too fast to allow the formation of closed 'hat'-like cones. Only further investigation of the fabrication of BN cones could help settle this issue, which is important in determining the viability of BN fullerene analogues.

The presence of a screw operation in the disclination also allows one to better understand how BN cones can grow so large along their cone-axis direction. Graphitic like flakes are known to grow much faster along their basal planes than along the stacking direction. Hence, a particularly efficient growth mechanism must be at play to yield particles that are larger in their c direction than along their basal planes. This may be the reason why BN and carbon cones modelled as a helically wound sheet (present work; Amelinckx *et al.*, 1992, respectively) contain many more stacked layers than the non-helical carbon cones associated with $60n^\circ$ disclinations (Krishnan *et al.*, 1997). Alternatively, one cannot exclude the possibility that different growth rates between the two types of cones be responsible for the different aspect ratios.

5. Conclusions

Hexagonal boron nitride cones have been observed by transmission electron microscopy for the first time. They were found to exhibit a high degree of two-dimensional order and weak intersheet correlations. The cone apex angles measured from the diffraction patterns were restricted to the 84 to 130° range, with the great majority of values located between 84 and 107°. A conical helix model was proposed to explain the multitude of cone-angle values. Analysis of the fine structure of the diffraction patterns gave corroborating evidence in support of the model. Although the conical helix structure is also observed in graphitic cones, preferred cone-angle values differ between the carbon and BN systems. The marked preference for apex angles close to 84°, where the disclination defect is a square ring, led us to the conclusion that the square was indeed the most favourable ring defect in hexagonal boron nitride. However, the very small number of BN cones with 120° disclinations still leaves unresolved the issue regarding the stability of square rings.

LB wishes to acknowledge the support of the Center of Excellence Project at the National Institute for Research in Inorganic Materials at Tsukuba, Japan.

References

Amelinckx, S., Devouard, B. & Baronnet, A. (1996). *Acta Cryst.* A**52**, 850–878.

Amelinckx, S., Luyten, W., Krekels, T., Van Tendeloo, G. & Van Landuyt, J. (1992). *J. Cryst. Growth*, **121**, 543–558.

Bacon, R. (1960). *J. Appl. Phys.* **31**, 283–290.

Banhart, F., Zwanger, M. & Muhr, H.-J. (1994). *Chem. Phys. Lett.* **231**, 98–104.

Blase, X., Rubio, A., Louie, S. G. & Cohen, M. L. (1994). *Europhys. Lett.* **28**, 335–340.

Bourgeois, L., Bando, Y., Shinozaki, S., Kurashima, K. & Sato, T. (1999). In preparation.

Chopra, N. G., Luyken, R. J., Cherrey, K., Crespi, V. H., Cohen, M. L., Louie, S. G. & Zettl, A. (1995). *Science*, **269**, 966–967.

Double, D. D. & Hellawell, A. (1974). *Acta Metall.* **22**, 481–487.
Golberg, D., Bando, Y., Eremets, M., Takemura, K., Kurashima, K. & Yusa, H. (1996). *Appl. Phys. Lett.* **69**, 2045–2047.
Haanstra, H. B., Knippenberg, W. F. & Verspui, G. (1972). *J. Cryst. Growth*, **16**, 71–79.
Hamilton, E. J. M., Dolan, S. E., Mann, C. M., Colijn, H. O., McDonald, C. A. & Shore, S. G. (1993). *Science*, **260**, 659–661.
Hubáček, M. & Sato, T. (1995). *J. Solid State Chem.* **114**, 258–264.
Iijima, S. (1991). *Nature (London)*, **354**, 56–58.
Ishii, T., Sato, T., Sekikawa, Y. & Iwata, M. (1981). *J. Cryst. Growth*, **52**, 285–289.
Jensen, F. & Toftlund, H. (1993). *Chem. Phys. Lett.* **201**, 89–96.
Krishnan, A., Dujardin, E., Treacy, M. M. J., Hugdahl, J., Lynum, S. & Ebbesen, T. W. (1997). *Nature (London)*, **388**, 451–454.
Kroto, H. W., Heath, J. R., O'Brien, S. C., Curl, R. F. & Smalley, R. E. (1985). *Nature (London)*, **318**, 162–163.
Loiseau, A., Willaime, F., Demoncy, N., Hug, G. & Pascard, H. (1996). *Phys. Rev. Lett.* **76**, 4737–4740.
Rubio, A., Corkill, J. L. & Cohen, M. L. (1994). *Phys. Rev. B*, **49**, 5081–5083.
Sato, T. (1996). *Research Report of NIRIM*, ch. 3, Vol. 89, pp. 12–13. NIRIM, Tsukuba, Japan.
Seifert, G., Fowler, P. W., Mitchell, D., Porezag, D. & Frauenfeim, Th. (1997). *Chem. Phys. Lett.* **268**, 352–358.
Shimomura, J., Funahashi, T. & Koitabashi, T. (1995). *J. Mater. Sci.* **30**, 3193–3199.
Stéphan, O., Bando, Y., Dussarrat, C., Kurashima, K. & Tamiya, T. (1997). *Proc. Electron Microscopy and Analysis Group Conf. EMAG97, Cambridge*, pp. 367–370. *Inst. Phys. Conf. Ser.* No 153, Section 8. Bristol: IOP.